Vibration-induced slip in sheared granular layers and the micromechanics of dynamic earthquake triggering. Supplementary Materials.

M. Griffa,[1,*] E.G. Daub,[2,3] R.A. Guyer,[2] P.A. Johnson,[2] C. Marone,[4,5] and J. Carmeliet[6,1]

[1] *Laboratory for Building Science and Technology, Swiss Federal Laboratories for Materials Science and Technology, EMPA, Überlandstrasse 129, CH-8600, Dübendorf, Switzerland*

[2] *Solid Earth Geophysics Group, Los Alamos National Laboratory, MS D443, NM 87545, Los Alamos, USA*

[3] *Center for Nonlinear Studies, Los Alamos National Laboratory, MS B258, NM 87545, Los Alamos, USA*

[4] *Dept. of Geosciences, Pennsylvania State University, PA 16820, State College, USA*

[5] *G3 Center and Energy Institute, Pennsylvania State University, PA 16820, State College, USA*

[6] *Chair of Building Physics, Swiss Federal Institute of Technology Zürich, ETHZ, CH-8093, Zürich, Switzerland*

(Dated: August 12, 2011)

Abstract

Supplemental Materials associated to the article with the same title. Section I contains details about the 2D Molecular Dynamics (MD) model used for the simulations. Section II shows similar results as within the article for the temporal evolution of macroscopic variables and the spatial distribution of non-affine deformation, related to another time interval of analysis and series of stick-slip events. Sections III and IV address the intrinsic irregularity of the simulated stick-slip dynamics, compared to the laboratory experiments. Finally, Section V contains a detailed explanation of the animated movies that can be downloaded from the same repository and complement the figures in the article and herein.

I. DETAILS ABOUT THE 2D MD MODEL

The 2D Molecular Dynamics (MD) model was developed and implemented by the Open Source code ESyS-Particle, ver. 2.0. ESyS-Particle is a software package for particle-based numerical modelling. The software implements the Discrete Element Method (DEM), a type of Molecular Dynamics technique widely used for modelling processes involving large deformations, granular flow and/or fragmentation. ESyS-Particle is designed for execution on parallel supercomputers, clusters or multi-core PCs running a Linux-based Operative System. ESyS-Particle has been under development at the Earth Systems Science Computational Centre, University of Queensland, Brisbane, Australia, and at the RWTH Aachen University, Aachen, Germany.

As dimensional units within the model we considered $L_0 = 150$ μm, $t_0 = 1$ s and $M_0 = 1$ kg, respectively for length, time and mass. Each variable and parameter is thus expressed in these units or combinations of them.

The driving block of the model (Fig. 1(a) of the article, top part) comprises a top layer of uniform particles, each one with radius equal to 1. Below that 1D lattice there is a layer of particles with size distribution within the range $[0.3; 1.0]$. All of these particles interact among themselves via a pseudo-tensorial spring having a compressional/extensional component, a shear one and finally a bending term. All of these components are expressed as Hookean springs. For the formulation of the correspondent elastic forces we specifically refer to Ref.[1] and to the notation used therein. Having in mind Eq. 1 of Ref.[1], the springs' elastic constants have values

$$\begin{aligned} K_r &= 2.9775 \cdot 10^7 \\ K_s &= 2.25 \cdot 10^5 \\ K_b &= 2.79 \cdot 10^5, \end{aligned} \tag{1}$$

respectively for the compressional/tensional spring, with radial/normal direction, passing through the centers of the two interacting particles, the shear/tangential spring (orthogonal to the radial direction) and the bending spring. Each resultant elastic bond can be broken only when a certain condition is satisfied (see Eq. 11 of Ref.[1]). This condition depends upon some threshold parameters, each of which is associated to a single type of spring. We set up these threshold values such that no bond broke during each of our simulations.

The substrate block (Fig. 1(a) of the article, bottom part) is the mirror image of the driving block in respect of the horizontal axis passing through the center of the granular layer. All of its particles have the same size distribution and properties of those of the drive block.

The granular layer (Fig. 1(a) of the article, center part) is made of particles with size distribution within the range $[0.7; 1.1] = [105; 165]$ μm, approximately corresponding to the same size range of the glass beads used as model fault gouge in the experiments by Johnson *et al.* (see the "Methods" section of Ref.[2] where the authors report a size range of $[105; 150]$ μm). The granular layer particles interact with each other only when they get in contact with each other, meaning, they are not bonded. The contact force has a radial/normal component simply given by the repulsive part of the same radial/normal Hookean component of the bonding force. However, in this case the respective spring stiffness constant has value $K_r = 5.954 \cdot 10^7$. Each contact force has also a tangential component which represents the inter-particle friction force. Its formulation is conceptually similar to the one of Cundall *et al.*[3] but implemented in a different way that allows to describe more accurately the transition from static friction to dynamic friction[4]. This different implementation comes at the cost of longer computational time.

In the specific case of our simulations the parameters associated to the frictional force are

$$\begin{aligned} K_s &= 5.954 \cdot 10^7 \\ \mu_s &= \quad 0.6 \\ \mu_d &= \quad 0.6, \end{aligned} \tag{2}$$

where K_s is the shear stiffness and μ_s/μ_d the static and dynamic friction coefficients, respectively. The interaction between one particle of the granular layer and one particle of the driving block or of the substrate block is described by the same contact/friction force between two particles of the granular layer. Finally, an artificial viscous bulk force was applied to each particle of the model to avoid the build up of kinetic energy inside the system due to its finite size along the vertical (Y-)axis.

The ESys-Particle MD code exploits a novel formulation for representing relative rotations of bonded particles. This formulation decomposes the relative rotation between two bonded particles into two sequence-independent rotations[1]. Thus, torques caused by rela-

tive rotations are uniquely determined because overall torsional and rolling angles can be distinguished. This formulation is based upon the use of quaternion algebra. It's a formulation that preserves the sequence-dependency of composed finite rotations and is numerically more stable compared to standard incremental methods[5,6].

Newton's equations of motion for the center of mass of each particle are solved using a velocity Verlet finite difference scheme while, for the correspondent rotational degrees of freedom, with a finite difference rotational leapfrog algorithm[6]. The temporal finite difference time step $\Delta t = 2.5 \cdot 10^{-5}$ was small enough to guarantee numerical stability and to satisfy the Sampling Theorem for a vibration signal with maximum frequency $f_{max} = 20$ kHz. This frequency value is indicatively the maximum sound frequency of vibration in the experiments by Johnson *et al.*[2].

The granular layer thickness in our model is approximately identical to the one in the reference experimental configuration, *i.e.*, approximately 3 mm.

The boundary conditions are periodic in X direction in order to approximate the simulation of a granular layer with large aspect ratio in shear direction without the need of very long computation time. In Y direction, the boundary conditions consist of a modified version of the constant normal force/stress boundary condition adopted by Aharonov *et al.*[7]. A similar implementation was used by Capozza *et al.* in their study of the effects of vibration on granular stick-slip[8]. Each simulation run consists in a first consolidation stage, 10000 simulation time steps long, when no shear load is imposed. During this initial time interval, the granular layer is simply compressed and dilated, displacing vertically both the top of the driving block and the bottom of the substrate, under the condition of achieving a constant normal load $\sigma_n = 600 \approx 4\ MPa$ exerted by the granular layer on both the drive block and the substrate. This condition always results in a transitory regime for the system's thickness in Y, during which it decreases approximately exponentially towards a steady state value. This equilibrium value is always achieved well before the end of the consolidation stage, guaranteering that the system is in complete steady state when the shear load starts to be applied. At the end of the consolidation phase, the position of the substrate bottom is recorded and kept fixed in time during every reference run and it is adopted as center value about which the Y displacement is imposed during the perturbed runs. The top of the drive block is still subject to the same constant normal load, all the time in each run, resulting in small amplitude displacement fluctuations about the steady state value achieved during

consolidation, as a consequence of dilation/compaction of both the granular layer and the substrate/drive block. Shear load is imposed starting at the end of the consolidation stage, initially with a linearly increasing speed till the wanted value $V_{X,0}$ is achieved (piece-wise linear ramp loading). This implementation of a constant normal stress in Y differs from previous ones for the vertical symmetry break. While the effective normal stress on the top of the drive block is constant, the one on the bottom of the subtrate fluctuates about an average value corresponding to the wanted σ_n. The fluctuation amplitude remains relatively small during each run, both reference and perturbed ones. For example, regarding the time interval $[1.45; 1.96]$ of Fig. 2 in the manuscript, the largest fluctuation amplitude (peak-to-peak), relative to the average value σ_n, is $\frac{\Delta\sigma_{n,PP}^{max}}{\sigma_n} \cong 8.79\%$ in the reference run and $\frac{\Delta\sigma_{n,PP}^{max}}{\sigma_n} \cong 8.49\%$ in the perturbed one. Vibration only changes the phase of the fluctuations but not the amplitude range.

We notice that some particles of the granular layer are squeezed out of their initial region during the consolidation stage. The driving block/substrate do not fully extend up to the lateral boundaries along Y, at the extremities of the system. As a consequence of periodic boundary conditions in X and of consolidation, some granular particles are squeezed below and above the line of the substrate/driving block and get trapped in between two sides of each of them. These "columns" of particles can be clearly observed in Fig. 3 of the manuscript and Fig. S2 here.

II. SIMULATION PHENOMENOLOGY FOR OTHER TIME INTERVALS OF ANALYSIS AND STICK-SLIP CYCLES.

This Section contains additional results showing that the phenomenology observed for the time interval and series of stick-slip cycles considered in the article is also observed during other time intervals, for a larger number of successive stick-slip cycles, in absence or presence of externally applied vibration.

One characterizing feature of the numerically simulated stick-slip dynamics consists in a low degree of correlation between the friction coefficient drop, $|\Delta\mu_f|$, and the thickness change, $|\Delta T|$, during slip. This feature is qualitatively evident from Figs. 2(b)-(d) in the article and from Figs. S1(b)-(d) below. For example, the slip event within the time interval $[1.46; 1.56]$ shown in Fig. 2(d) of the article happens with almost no thickness drop (no

compaction), both for the reference and for the perturbed runs. The same is true for the slip event within the time interval $[10.06; 10.16]$ of Fig. S1(d), which is analogous to Fig.2(d) of the article but refers to another time range. In both cases the figures refer to, it is possible to notice that some slip events are accompanied by compaction, others are not and there is a low level of correlation between the friction coefficient drop amplitude and the thickness drop one.

The second main characteristic feature of the numerically simulated stick-slip dynamics consists in the similarity of the patterns of temporal evolution for the non-affine deformation metric $M(\bar{r}, t)$ defined within the article. Prior to slip M assumes small values almost everywhere, homogeneously, across the granular layer, except for small and isolated regions where it departs from 0 mainly due to single particles acting like rattlers. At the onset of rapid slip, M undergoes a sudden increase in a very localized region of the top of the granular layer, close to the drive block. Later on, M's localized peak values disappear and non-affine deformation spreads more widely within the bulk of the granular layer, achieving larger values than before the onset of slip. This type of pattern for the spatial-temporal evolution of M during stick-slip is evident in Fig. 3 of the article and in Fig. S2 below.

Figure S2 refers to the same couple of reference/perturbed simulations Fig. S1 is associated with. The reference simulation is the same as the one described within the article. The perturbed simulation consists in applying external vibration of the same type as described within the article but during the time interval $[10.06; 10.16]$. It is important to remark that vibration amplitude, frequency, duration and modulation are the same as cited in the article. Figures S2 (a), (c) and (e) refer to three different times during a stick-slip cycle of the reference run. The symbols within each inset help to identify which friction coefficient state the figures refers to (see Fig. S1 for comparison). These three figures show another example of spatially localized increase of non-affine deformation during slip. Compared to the stick-slip cycle analyzed in the article, in this case there are less rattlers, thus no visible circular spots of slightly-above-average non-affine deformation during the stick period (Fig. S2(a)). Non-affine deformation increases abruptly within two different and separated regions of the shear zone (Fig. S2(c) and (e) respectively), at different times. Remarkedly, the two highly non-affine spots corresponds to two different peak values for $< M > (t)$ in Fig. S1(e).

Figures S2 (b), (d) and (f) refer to three different moments during the same stick-slip phase when perturbed by vibration, applied during the time interval $[10.06; 10.16]$. They

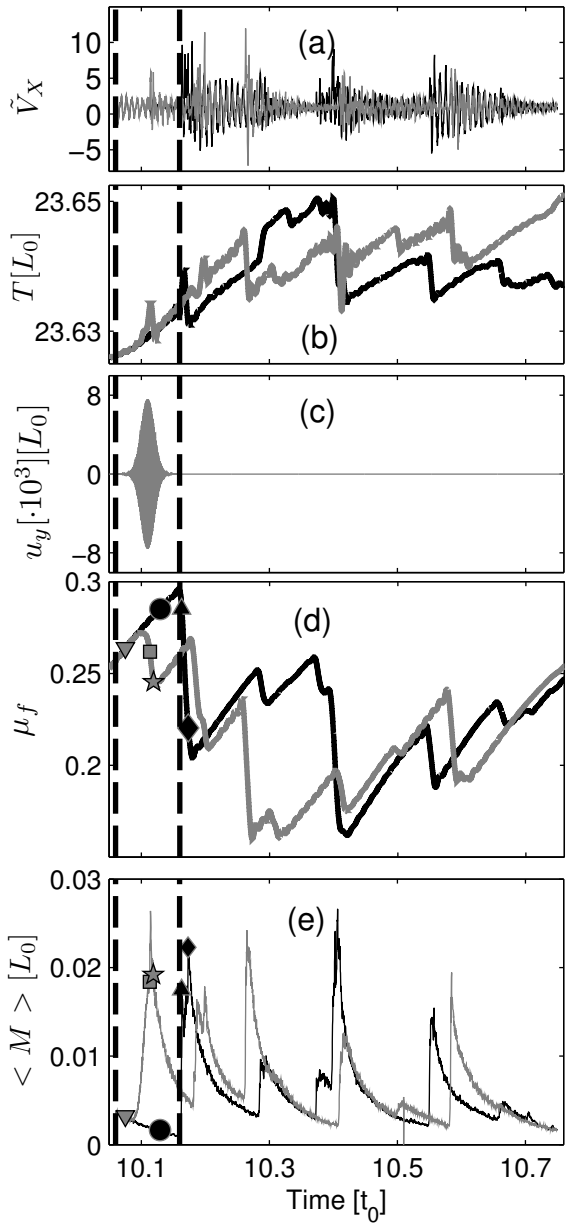

Figure S 1. Macroscopic signals for a couple of runs identical to the ones described in the article except for the time interval when external vibration is used for the perturbed run, in this case being $[10.06; 10.16]$. (a) Normalized driving block's Center Of Mass (COM) velocity along the shear direction (X-axis), $\tilde{V}_X$. (b) Model's thickness in Y, T. (c) Substrate's bottom displacement in Y direction, u_y, for the perturbed run. (d) Friction coefficient of the interface between the granular layer and the driving block. For the meaning of the symbols, see Fig.S2. (e) Granular layer ensemble average of the non-affine deformation metric M. The vertical dashed lines in all the insets outline the time interval of interest, when vibration is imposed. Black lines refer to the reference run, in absence of vibration. Gray lines refer to the perturbed case, with applied vibration.

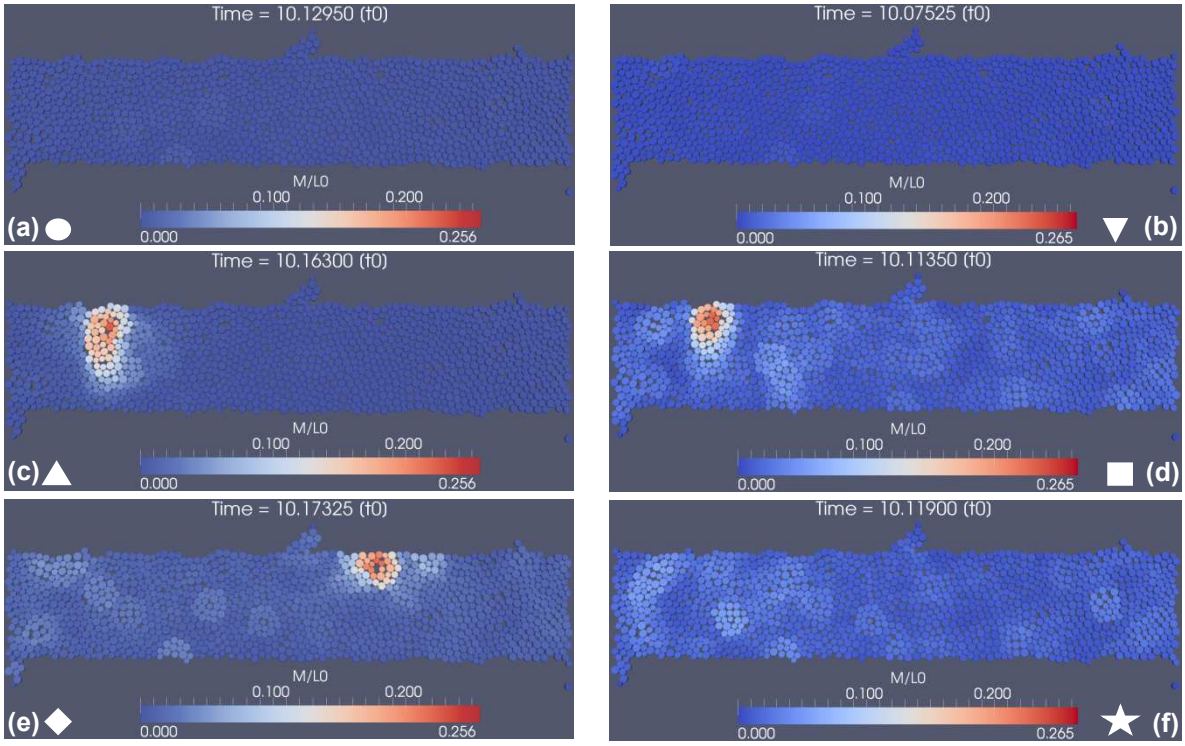

Figure S 2. Non-affine deformation metric map, $M(\bar{r}, t)$, at different times (see corresponding identifying symbols in Fig. S1). Simulation runs where the externally applied vibration occurs this within the interval $[10.06; 10.16]$. (a), (c), (e): reference run, without applied vibration. (b), (d), (f): perturbed run, with applied vibration. Only granular layer particles are visualized. Each of them is labeled with a color value corresponding to the local M value. See Section V for corresponding animated movies showing the temporal evolution of $M(\bar{r}, t)$ during the time interval $[10.06; 10.16]$, for both the reference and perturbed runs.

confirm the similarity between a "spontaneous" slip and a dynamically triggered one, in terms of evolution of the non-affine deformation pattern.

We performed other couples of simulations like this one, just varying the beginning time of vibration application, and got results that confirm the phenomenology described in the article and herein.

III. REGULAR VS IRREGULAR STICK-SLIP DYNAMICS. COMPARISON WITH LABORATORY EXPERIMENTS.

The irregularity that accompanies the numerically simulated stick-slip dynamics represents a key difference compared to the extreme regularity of the double-axial shear experiment performed at Penn State University's Rock and Sediment Mechanics Lab by Johnson *et al.*[2]. One example of irregularity consists in the relation between the friction coefficient drop $\Delta\mu_f$, associated with each slip event, and the corresponding change in thickness ΔT. Figure S3 is the scatter plot of $|\Delta\mu_f|$ *vs* $|\Delta T|$ for a lab experiment, in absence of applied vibration. Figure S4 is a similar plot but for our simulated reference run, considering the population of 150 identified slip events that are accompanied by compaction ($\Delta T > 0$). The comparison of the two figures clearly shows that in the experimental case there is almost linear correlation between the two variables (linear correlation coefficient $R = 0.9419$), *i.e.*, large slip events (in terms of friction coefficient drop) occur with large compaction. The simulated reference run exhibits a smaller degree of correlation.

In the experiment, the size of the slip event, still in terms of friction coefficient drop, is almost constant, as shown in Fig. S5, reporting the probability that the friction coefficient drop, $\Delta\mu_f$, as a random variable, assumes values greater than or equal to $\Delta\mu_f'$. This probability has been calculated using the catalog of 264 slip events identified in the experimental dataset and it represents $1-$ the Cumulative Distribution Function of $\Delta\mu_f$. The blue, dashed line corresponds to a maximum likelihood-based power law best fitting of part of the curve according to the method of Clauset *et al.*[9]. The best fitting has been performed for the range $\Delta\mu_f \geq 0.0974$. The experimental dataset essentially contains only large size slip events that follows a power law, *i.e.*, Gutenberg-Richter-like, statistics.

In the simulation, the reference run exhibits a large range of slip friction coefficient drops. Figure S6 shows the same type of probability for the friction coefficient drop, $\Delta\mu_f$, as a random variable, using this time as statistical ensemble the values determined from the catalog of about 150 slip events happening with compaction. The dashed line still corresponds to the same type of maximum likelihood-based power law best fitting of part of the curve according to Ref.[9]. The maximu likelihood-based best fit shows that only the tail of the distribution, consisting in large slip events, follows a power-law (Gutenberg-Richter-like) behavior while smaller events are characterized by other statistical properties. This

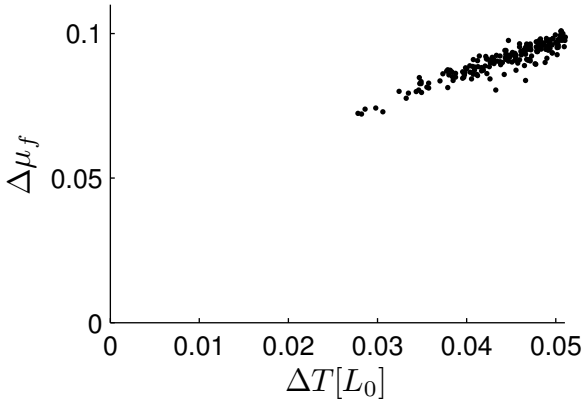

Figure S 3. Friction coefficient drop, $|\Delta\mu_f|$, *vs* thickness change, $|\Delta T/L_0|$, during slip, calculated for a double-axial shear experiment in the absence of applied vibration. The experiment was a run similar to the one described in Ref.[2], with a normal load of 5 MPa. For this figure, we considered a population of 264 slip events. The linear correlation coeffient between $|\Delta\mu_f|$ and $|\Delta T|$ for this dataset is $R = 0.9419$.

result stems from the larger degree of irregularity of stick-slip dynamics in our simulation, compared to the experiments of Johnson et al.[2], and is typical of both Earth and laboratory catalogs of slip events[10,11].

The difference between the experimental CDF and the simulation one is expected and is in agreement with results from field observations[12,13]. Indeed, being almost completely regular, the experimental stick-slip dynamics covers only a small range of slip friction drop values. At this small friction drop scale, a power law-like Probability Density Function can be approximately described by a log-normal one[10,14], which leads to the type of CDF shown in Fig. S5. On the contrary, the simulation stick-slip dynamics is more irregular and involves a larger range of friction coefficient drop values, thus a more remarked power law-like distribution.

One reason for this key difference between our numerical simulation and the experiments consists in the fact that the experimental configuration was fine tuned in order to obtain a high degree of regular stick-slip dynamics while we did not fine-tune as well the parameters of our MD simulations. In this work, we wanted to achieve stick-slip behavior closer to the field reality, in terms of variability[11].

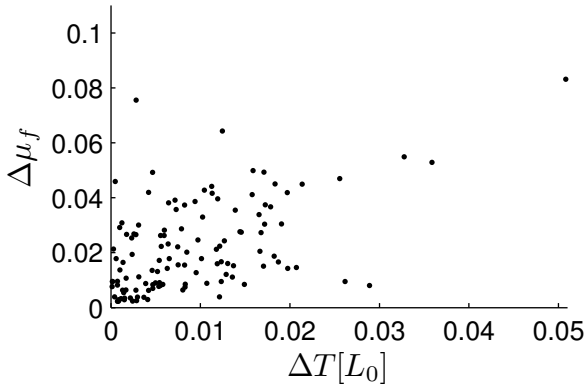

Figure S 4. Friction coefficient drop, $|\Delta\mu_f|$, *vs* thickness change, $|\Delta T|$, during slip, calculated for the reference run out of a population of 150 slip events within the time interval $[1; 25]$. The thickness change associated with a slip event was calculated as the thickness at the slip onset - thickness at its end. The linear correlation coeffient between $|\Delta\mu_f|$ and $|\Delta T|$ is $R = 0.5109$.

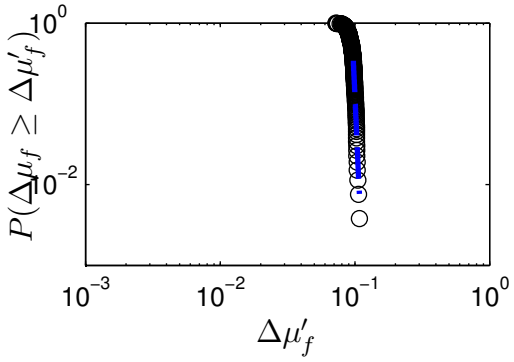

Figure S 5. Probability that the friction coefficient drop, $\Delta\mu_f$, as a random variable, assumes value greater than or equal to $\Delta\mu'_f$, using as statistical ensemble the values determined from the experimental run catalog of about 264 slip events. The blue, dashed line corresponds to a maximum likelihood-based power law best fitting of part of the curve according to the method of Clauset *et al.*[9]. The part of the dataset corresponding to a power law behavior, *i.e.*, to a Gutenberg-Richter like slip event distribution, is $\Delta\mu'_f \geq 0.0974$.

IV. ANALYSIS OF SLIP EVENTS ACCOMPANIED BY NO COMPACTION.

The second source of difference with the experimental results about the $(|\Delta\mu_f|, |\Delta T|)$ correlation is intrinsically due to one of the main features of our model, *i.e.*, the use of deformable drive/substrate blocks. We performed a detailed analysis of the particle rear-

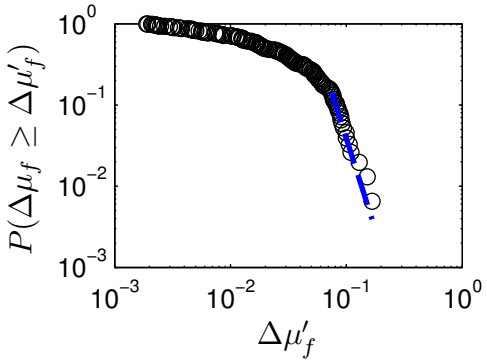

Figure S 6. Probability that the friction coefficient drop, $\Delta\mu_f$, as a random variable, assumes value greater than or equal to $\Delta\mu'_f$, using as statistical ensemble the catalog of about 150 slip events happening with compaction in the reference run. The dashed line corresponds to a maximum likelihood-based power law best fitting of part of the curve according to the method of Clauset *et al.*[9]. The part of the dataset corresponding to a power law behavior, *i.e.*, to a Gutenberg-Richter like slip event distribution, is $\Delta\mu'_f \geq 0.075$.

rangement during some of the slip events occuring without compaction. In this analysis, we looked at animated movies of the particle assemblies during the slip events. These movies show that limited parts of the granular layer and of the drive block undergo significant deformations during such slip events. Being the overall thickness of the system, T, calculated by the lowest and highest drive block/substrate particle positions along the $Y-$ axis, a slip event may induce more local bending of the bonded particle assemblies and less rigid-body vertical shift, thus producing almost no thickness change.

V. SPATIO-TEMPORAL EVOLUTION OF NON-AFFINE DEFORMATION: ANIMATED MOVIES.

The movie file **ReferenceRun.avi** refers to the reference simulation, the one without applied vibration. This movie shows a series of frames, each one containing two insets. The bottom inset contains the plot of the friction coefficient *vs* time, within the time interval $[1.46; 1.56]$. For comparison, see Fig. 2(d) within the article. The square symbol moving along the curve in the plot identifies the time instant and the corresponding friction coefficient value when a snapshot of the non-affine metric function M is shown in the top inset.

These snapshots are analogous to the ones of Fig. 3 within the article. The two insets allow for comparing the temporal evolution of the friction coefficient (macroscopic variable) with the temporal evolution of the spatial distribution of the non-affine deformation level, provided by M (mesoscopic variable).

The movie file **PerturbedRun.avi** is analogous to **ReferenceRun.avi** but it refers to the perturbed simulation, the one with applied vibration within the time interval $[1.46; 1.56]$. The bottom inset shows the plot of the friction coefficient *vs* time (gray line) for the perturbed run along with the same plot for the reference run (black line). The M snapshots (top inset) refer only to the perturbed run.

The movie files **ReferenceRun2.avi** and **PerturbedRun2.avi** are of the same type as the previous two but refer to the case of vibration applied within the time interval $[10.06; 10.16]$. See Fig. S1 for the corresponding temporal evolution of macroscopic variables for this couple of simulations.

For every animated movie, the time gap between two consecutive frames corresponds to 10 simulation time steps, *i.e.,* $2.5 \cdot 10^{-4}$. The frame rate of each movie is 7 fps. Each movie was compressed by a JPEG encoder. Corresponding movies are available also in PNG format at the the same Web page.

---

* michele.griffa@empa.ch

[1] Y. Wang, S. Abe, S. Latham, and P. Mora, Pure Appl. Geophys. **163**, 1769 (2006).

[2] P. A. Johnson, H. Savage, M. Knuth, J. Gomberg, and C. Marone, Nature **451**, 57 (2008).

[3] P. Cundall and O. Strack, Geotechnique **29**, 47 (1979).

[4] D. Place and P. Mora, J. Comp. Phys. **150**, 332 (1999).

[5] Y. Wang and F. Alonso-Marroquin, Granular Matter **11**, 331 (2009).

[6] Y. Wang, Acta Geotech. **4**, 117 (2009).

[7] E. Aharonov and D. Sparks, Phys. Rev. E **60**, 6890 (1999).

[8] R. Capozza, A. Vanossi, A. Vezzani, and S. Zapperi, Physical Review Letters **103**, 085502 (2009).

[9] A. Clauset, C. Shalizi, and M. Newman, SIAM Rev. **51**, 661 (2009).

[10] M. Newmann, Contemp. Physics **46**, 323 (2005).

[11] M. Bretz, R. Zaretzki, S. Field, N. Mitarai, and F. Nori, Europhys. Lett. **74**, 1116 (2006).

[12] B. Allmann and P. Shearer, J. Geophys. Res. **112**, B04305 (2007).

[13] B. Allmann and P. Shearer, J. Geophys. Res. **114**, B01310 (2009).

[14] M. Mitzenmacher, Internet Math. **1**, 226 (2003).